



Tri-templates synthesis of SAPO-34 and its performance in MTO reaction by statistical design of experiments



Shima Masoumi^a, Jafar Towfighi^{a,*}, Ali Mohamadalizadeh^{b,c}, Zahra Kooshki^a, Kobra Rahimi^a

^a Department of Chemical Engineering, Tarbiat Modares University, Chamran Highway Ale-Ahmad Cross, P.O. Box 14115-143, Tehran, Iran

^b Gas Research Division, Research Institute of Petroleum Industry, Tehran 14665-1998, Iran

^c Department of Chemical Engineering, Polytechnique Montreal, Succ. Centre-ville, Montréal, Québec H3C 3A7, Canada

ARTICLE INFO

Article history:

Received 3 September 2014
Received in revised form
16 December 2014
Accepted 18 December 2014
Available online 8 January 2015

Keywords:

MTO reaction
Light olefin
SAPO-34
Tri-templating
Central composite design

ABSTRACT

The effect of a tri-templating agent [i.e., tetraethyl ammonium hydroxide (TEAOH), triethylamine (TEA) and morpholine (MOR)] on the catalytic performance of SAPO-34 catalyst was investigated in conversion of methanol to olefins (MTO). SAPO-34 catalysts were synthesized hydrothermally with nominal composition as $1 \text{Al}_2\text{O}_3 : 1 \text{P}_2\text{O}_5 : 0.4 \text{SiO}_2 : 2y \text{TEAOH} : 2x \text{TEA} : 2(1 - (x + y)) \text{MOR} : 70 \text{H}_2\text{O}$. The products were characterized by XRD, SEM, BET, EDX, FT-IR, NH_3 -TPD techniques. The relative molar ratios were obtained by response surface methodology applying central composite design. Tri-templating led to production of pure SAPO-34 phase with reduced particle sizes. Analysis of Variance (ANOVA) applied for investigating the significance of two independent variables indicated that TEA content was the most significant variable. The catalytic performance of the prepared catalysts was tested in MTO reaction at 410 °C and WHSV of 6.5 h⁻¹. Sample prepared with 0.5 MOR:0.5 TEA:1 TEAOH exhibited the highest yield of light olefins (88.7 wt%) owing to its highest crystallinity, smallest crystal size and highest surface area.

© 2015 Elsevier B.V. All rights reserved.

1. Introduction

Ethylene and propylene are the most important raw materials in petrochemical industries used for production of major chemicals [1,2]. The main source of these chemicals is steam cracking of gas and liquid hydrocarbons at high temperature, but this method demands an appreciable amount of energy with concomitant environmental problems such as CO₂ emissions and also has high production cost due to high crude oil price [3,4].

Nowadays, research interest has been focused on methanol to olefins (MTO) process because of the availability of huge quantities of natural gas and an increasing public awareness for providing raw materials from natural gas [5,6]. There have been many molecular sieve catalysts applied for the MTO reaction [7–9]. SAPO-34, has received great attention due to relatively mild acidity, chabazite structure, good thermal/hydrothermal stability and high selectivity to olefins in MTO reaction [10,11]. SAPO-34 is formed by the introduction of silicon atoms into the neutral framework of aluminophosphate (ALPO₄) molecular sieve, which causes a negative

imbalance in the framework's charge then creation of Bronsted acid sites [12–15].

SAPO-34 is normally synthesized hydrothermally from a gel containing sources of Al, Si and P. Also, one or a mixture of components is added to reacting mixture as structure directing agents (SDA) [16–18]. It is well known that template can play structure-directing, space-filling, and charge-compensating roles in the synthesis of SAPO molecular sieves [19–21].

Alvaro-Munoz et al. [22] used different templates such as tetraethyl ammonium hydroxide (TEAOH), triethylamine (TEA) and morpholine (MOR) in SAPO-34 synthesis. The sample synthesized with TEAOH as template rendered the best catalytic performance owing to its enhanced external surface area and stronger acidity, but its high price limits its application in an industrial scale. However, TEA and MOR cost considerably lower than TEAOH, but MOR had little effect on the nucleation so that accelerated the crystal growth of SAPO-34 resulting in large particle size and lower catalytic performance in MTO reaction [23]. On the other hand, TEA was reported to cause to the presence of impurity phase and small size particles [24,25].

Recently, mixed templates such as TEAOH/MOR [26,27] and TEAOH/TEA [28] have been employed in the synthesis of SAPO-34 in order to improve the properties of SAPO-34 and increase its catalytic performance. Although three kinds of amines, namely

* Corresponding author. Tel.: +98 21 82883311; fax: +98 21 82883311.

E-mail address: towfighi@modares.ac.ir (J. Towfighi).

TEAOH, TEA, MOR and a mixture of two these templates have been used as most common SDA in the synthesis gel, but the effect of different combinations of a new tri-template agent TEAOH/TEA/MOR has not been investigated.

In this work, central composite design (CCD) was applied to investigate how the ratios of TEA/TEAOH/MOR influence the characteristics of SAPO-34 as well as its catalytic performance in MTO reaction. Different samples were synthesized using two or three templates with different molar ratios of TEA/TEAOH/MOR in the starting gel. Analysis of Variance (ANOVA) was employed to study the effect of the main factors and the associated interaction on relative crystallinity and maximum yield of light olefins. A quadratic model was proposed for maximum yield of light olefins and relative crystallinity as a function of TEA and TEAOH content in synthesis gel. The crystal size, crystallinity, specific surface area, chemical composition and acidic properties of the samples were characterized by XRD, SEM, BET, EDX, FTIR and NH₃-TPD techniques. The reactor tests were performed over the prepared catalysts in order to obtain the best ratios of TEA/TEAOH/MOR in MTO reaction to find the proper catalyst for this reaction.

2. Experimental

2.1. Catalyst preparation

The SAPO-34 samples were synthesized hydrothermally using the mixture of three different organic templates namely, MOR (Merck), tetraethyl ammonium hydroxide (20 wt% aqueous solution of TEAOH, Merck) and TEA (Merck). Aluminum isopropoxide, silica gel and phosphoric acid (85 wt%, H₃PO₄, Merck) were used as the source of Al, Si and P, respectively. The molar composition of synthesis gel was 1 Al₂O₃:1 P₂O₅:0.4 SiO₂:2y TEAOH:2x TEA:(1-(x+y)) MOR:70 H₂O.

The synthesis gel was prepared by slowly adding aluminum isopropoxide powder to a solution containing phosphoric acid and deionized water with continuous stirring, then silica gel was added drop wise to the above solution, followed by addition of templates. The obtained gel was aged at room temperature for 8 h with agitation. After the aging period, the gel was transferred into a Teflon-lined stainless steel autoclave, which was heated at 190 °C for 24 h. The synthesized material was recovered by centrifugation, washed several times with distilled water, and then oven-dried at 110 °C for 10 h. The final product was calcined at 550 °C for 5 h in order to remove the organic templates that resided in the pores of the samples.

2.2. Catalyst characterization

The X-ray diffraction (XRD) patterns of catalysts were obtained by powder X-ray diffractometer (Bruker D8) using CuK α radiation ($\lambda = 1.54 \text{ \AA}$). For zeolite SAPO-34, the relative crystallinity was determined from the main peak intensities at $2\theta \approx 9.6, 13.0$, and 20.6 [29] on the base of SAPO-34 catalyst prepared with 0.5 MOR:0.5 TEA:1 TEAOH molar ratio possessing the highest XRD intensities among other samples. Therefore, the relative crystallinity of the samples was calculated by Eq. (1):

$$\% \text{ relative crystallinity} = \frac{\sum I}{\sum I_2} \times 100 \quad (1)$$

where I is the line intensity of the sample and I_2 is the line intensity of the S2 sample. The crystal size and morphology was analyzed using Philips XL30 scanning electron microscope (SEM). Diffuse reflectance FTIR was conducted using a Bruker Tensor-27 spectrophotometer. IR spectra of the samples in the region of the framework stretching vibrations (450–4000 cm⁻¹) were measured.

The BET specific surface areas of calcined samples were acquired from isotherm data of nitrogen adsorption–desorption at –196 °C using Micromeritics ASAP-2010 analyzer. The chemical composition of the catalysts was determined by TESCAN system (VEGA model) scanning electron microscope equipped with an energy dispersive X-ray (EDX) spectrometer. The catalyst acidic properties were measured by temperature programmed desorption of ammonia (NH₃-TPD) using Micromeritics 2000. About 0.06 g of the catalyst was pretreated to remove adsorbed water at 300 °C for 3 h and was subsequently cooled to the adsorption temperature of 100 °C. After purging with helium for 20 min, the analysis was carried out at a heating rate of 10 mL/min from 100 to 600 °C.

2.3. Catalyst performance test

Methanol conversion to olefins was tested under atmospheric pressure at 410 °C. The SAPO-34 catalyst weighing 1 and 2.5 g silicon carbide (as an inert) [30] were packed in the center of stainless steel reactor (internal diameter: 6 mm, length: 8 cm) and heated by a tubular furnace. The catalysts were pretreated with 150 mL/min flow of N₂ at 550 °C for 1 h and then the temperature was reduced to reaction temperature (410 °C).

The liquid mixture of methanol in water (30 wt%) with a weight hourly space velocity (WHSV) of 6.5 h⁻¹, was fed into the reactor. The gas product was analyzed by a Hewlett-Packard 5890 flame ionization detector (FID) gas chromatograph (GC) equipped with Agilent J&W GS-alumina and plot columns. The oven was operated at 50 °C, then ramped at 5 °C/min up to 180 °C and held for 5 min at 180 °C. Finally the temperature ramped to 50 °C at the same rate for the next test. The yield of products is defined by Eq. (2):

$$Y_p = \frac{m_{g(\text{out})} \times x_p}{m_{\text{MeOH}(\text{in})}} \times 100 \quad (2)$$

where in Eq. (2), Y_p is yield of product (wt%), $m_{g(\text{out})}$ is mass flow rate of outlet gas product, and x_p is mass fraction of product that were analyzed by GC, and $m_{\text{MeOH}(\text{in})}$ is mass flow rate of inlet methanol. The conversion of methanol was determined by Eq. (3), using fractional distillation of outlet liquid.

$$X_{\text{MeOH}} = \frac{(m_{\text{MeOH}(\text{in})} - m_{\text{MeOH}(\text{out})}) \text{ or (consumed method)}}{m_{\text{MeOH}(\text{in})}} \times 100 \quad (3)$$

where in Eq. (3), X_{MeOH} is conversion of methanol (%), $m_{\text{MeOH}(\text{in})}$ and $m_{\text{MeOH}(\text{out})}$ are the inlet and outlet mass flow rate of methanol, respectively.

2.4. Design of experiments

Central Composite Design (CCD) was applied to investigate the effect of two independent variables namely, TEA content (A) and TEAOH content (B) on relative crystallinity and maximum yield of light olefins. CCD method of experimental design and molar composition as 2x TEA:2y TEAOH:2 (1-(x+y)) MOR was used to find molar ratios of these templates. These two independent factors were coded as +1 for high level, 0 for center value, –1 for low levels and $\pm\alpha$ for axis point. The distance from the center of the design space to axial point is called α [31]. The five examined levels for each independent variable are shown in Table 1. The applied molar ratios of three templates are given in Table 2.

The effect of TEA and TEAOH content in synthesis gel on maximum yield of light olefins and relative crystallinity is explained

Table 1

Variables and their examined levels used in experimental design.

Factor	Level	Axis			
		-1	0	+1	- α
A - x (TEA content)	0.07	0.25	0.43	0	0.5
B - y (TEAOH content)	0.07	0.25	0.43	0	0.5

by the following quadratic polynomial equation as a function of independent variables is given in Eq. (4):

$$Y = \beta_0 + \sum_{i=1}^k \beta_i X_i + \sum_{i=1}^k \beta_{ii} X_i^2 + \sum_{i=1}^k \sum_{i < j} \beta_{ij} X_i X_j \quad (4)$$

where Y is the calculated response, k is the number of variables, β_0 is the constant coefficient, β_i is the linear coefficient, β_{ii} is the squared coefficient, β_{ij} is the interaction coefficient, X_i and X_j are uncoded independent variables.

Analysis of variance (ANOVA) utilized to investigate the significance of the main factors and their interactions is given in Tables 3 and 5. The significance of each factor is investigated using F and p values. Values less than 0.05 for p indicate that a variable is significant. The F test, is defined as $F = MSF/MSE$, where MSF and MSE are the mean squares of factors or interactions, and errors, respectively. The statistical significance of a factor is determined by comparison of the value in the F table at the desirable probability level (e.g., $F_{0.05}(9,7) = 2.53$) [31,32]. The greater value of F for each factor indicates that its effect is statistically significant.

3. Results and discussion

3.1. Crystallinity and crystal size (XRD, SEM)

The X-ray diffraction patterns of the synthesized catalysts prepared by different molar ratios of templates are shown in Fig. 1. The as-synthesized SAPO-34 exhibits a mixed trigonal and triclinic phase, whereas after calcination an exclusive trigonal phase is detectable [2]. As Fig. 1 shows diffraction peaks of trigonal phase appeared for all the samples.

All the synthesized samples possessed typical powder diffraction patterns corresponding to chabazite structure of SAPO-34 as

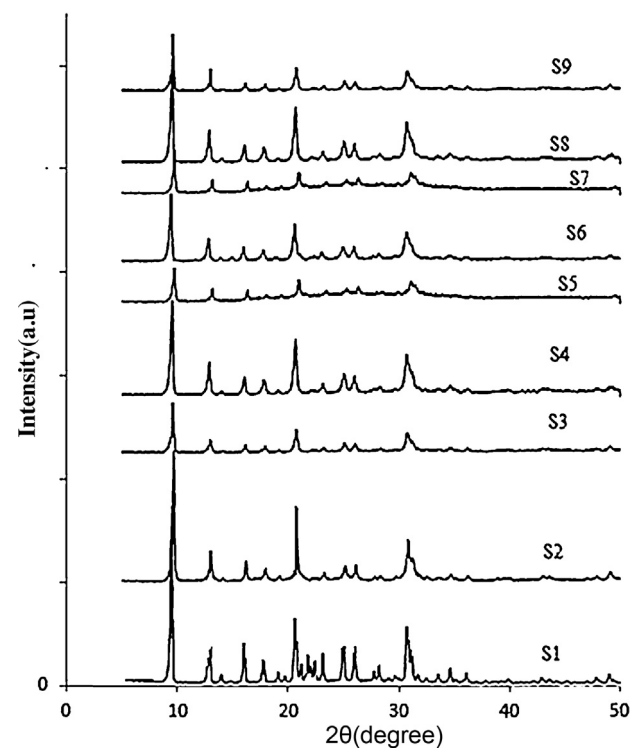


Fig. 1. XRD patterns of as-synthesized SAPO-34 with different molar ratios of templates.

seen in Fig. 1. The intensity and position of each peak match well with that of reported for SAPO-34 material without the presence of any impurity phase [29]. Furthermore, there is no additional peak of impurity phase in any of the samples implying that SAPO-34 was successfully crystallized. According to the XRD patterns, reflection intensities of each peak varied with changing molar ratios of

templates. The intensities of peaks associated with S2 sample prepared from a mixture of 0.5 MOR:0.5 TEA:1 TEAOH are the highest. It can be regarded as the base sample for determining the relative crystallinity of the other samples. The relative crystallinity of each catalyst are presented in Table 2.

According to ANOVA results for relative crystallinity, the factor A and interactions AB and A² were proved to have statistically significant effects on the relative crystallinity (Table 3).

After the ANOVA test, the quadratic polynomial equation for relative crystallinity as a function of actual variables is given in Eq. (5):

$$\begin{aligned} \text{Relative crystallinity}(\%) = & +62.05685 + 202.82944X_A + 85.14315X_B - 176.00000X_AX_B \\ & - 391.60000X_A^2 - 63.60000X_B^2 \end{aligned} \quad (5)$$

In which X_A and X_B denote actual variables of TEA and TEAOH content, respectively. Determination coefficient (R^2) of Eq. (5) is 0.92, indicating that this model can describe the experimental data of relative crystallinity.

Main effects of each factor on relative crystallinity are presented in Fig. 2. Increasing TEA content in synthesis gel led to increase in relative crystallinity initially, reaching to a maximum and then falling (Fig. 2(a)). The intensity of main peaks in the XRD pattern

Table 2

Molar ratios, relative crystallinity (%) and mean crystal size of SAPO-34 samples.

Samples	Molar composition	Relative crystallinity (%)	Mean crystal size (μm)
S1	Al ₂ O ₃ :0.4 SiO ₂ :1 P ₂ O ₅ :1.5 MOR:0.5 TEA	85	3.25
S2	Al ₂ O ₃ :0.4 SiO ₂ :1 P ₂ O ₅ :0.5 MOR:0.5 TEA:1 TEAOH	100	0.64
S3	Al ₂ O ₃ :0.4 SiO ₂ :1 P ₂ O ₅ :1.5 MOR:0.5 TEAOH	83	2.92
S4	Al ₂ O ₃ :0.4 SiO ₂ :1 P ₂ O ₅ :1 MOR:0.5 TEA:0.5 TEAOH	95	1.2
S5	Al ₂ O ₃ :0.4 SiO ₂ :1 P ₂ O ₅ :0.5 MOR:1 TEA:0.5 TEAOH	62	1.45
S6	Al ₂ O ₃ :0.4 SiO ₂ :1 P ₂ O ₅ :1 MOR:0.86 TEA:0.14 TEAOH	81	1.5
S7	Al ₂ O ₃ :0.4 SiO ₂ :1 P ₂ O ₅ :0.28 MOR:0.86 TEA:0.86 TEAOH	65	1.32
S8	Al ₂ O ₃ :0.4 SiO ₂ :1 P ₂ O ₅ :1 MOR:0.14 TEA:0.86 TEAOH	88	1.25
S9	Al ₂ O ₃ :0.4 SiO ₂ :1 P ₂ O ₅ :1.72 MOR:0.14 TEA:0.14 TEAOH	80	1.63

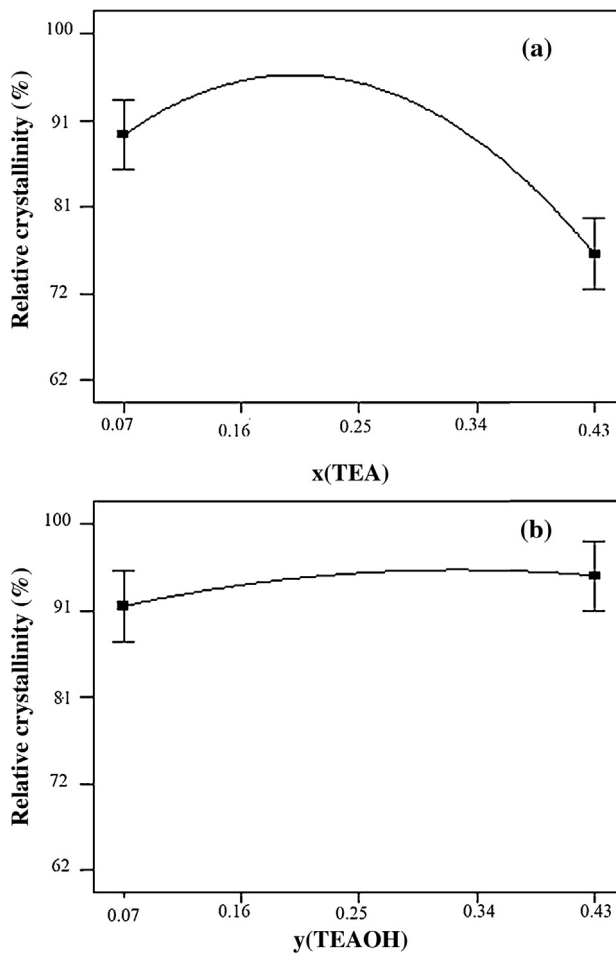
Table 3

Analysis of variance (ANOVA) for relative crystallinity (%).

Factor	Sum of squares	df	Mean square	F	p
Model	1527.40	5	305.48	15.46	0.0012
A – x (TEA content)	341.71	1	341.71	17.30	0.0042
B – y (TEAOH content)	21.82	1	21.82	1.10	0.3282
AB	121.00	1	121.00	6.12	0.0425
A^2	1041.78	1	1041.78	52.73	0.0002
B^2	27.48	1	27.48	1.39	0.2768
Error	1.20	4	0.30		
Core total	1665.69	12			

for S5 sample was weak. This sample exhibited the lowest relative crystallinity due to the highest amount of TEA content in synthesis gel. TEA content has the largest effect on the relative crystallinity. According to **Table 3**, the F values for A and A^2 that related to TEA content in synthesis gel are 17.30 and 52.73, respectively, which are much higher than other terms. These results are well reflected by **Fig. 2(a)** and (b). For instance, **Fig. 2(a)** shows that the increase of TEA changes the relative crystallinity in the range of 75–95% while **Fig. 2(b)** shows that the increase of TEAOH results in increasing of relative crystallinity in the range of 91–95%. These values confirm that TEAOH content does not have any significant effect on relative crystallinity in comparison with TEA.

Contour plots as the graphical representations that were obtained from Eq. (2), can be used to study the effects of process variables on the relative crystallinity. It is shown in **Fig. 3**, high level of TEAOH and low level of TEA content in the synthesis gel correlated with high relative crystallinity.

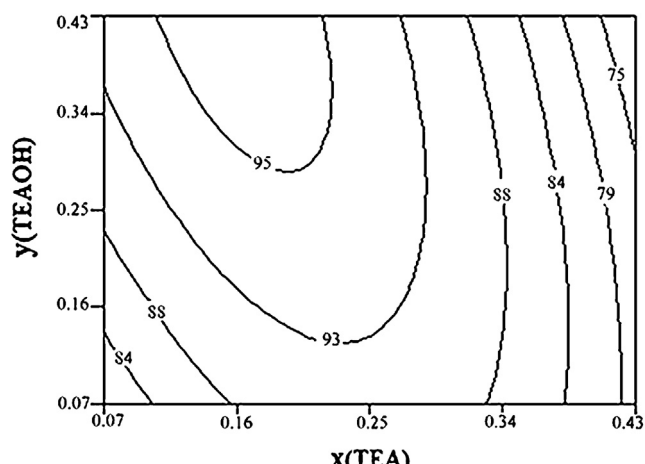
**Fig. 2.** Main effects of each factor on relative crystallinity (%).

Wang et al. [28] found that, when TEA template individually or a mixture of TEA/TEAOH is used to prepare SAPO-34, the SAPO-5 impurity phase could be also observed. XRD patterns confirmed that mixture of TEAOH/TEA/MOR can improve the purity of SAPO-34. So using MOR as a third template may help to obtain pure phase of SAPO-34.

The SEM images of the synthesized samples are presented in **Fig. 4**. All the samples exhibited the cubic shape of typical SAPO-34, distinct in crystal size. The SEM study confirmed that crystal size of samples depended on the type and number of templates in the initial gel. According to Refs. [23,24,26,33,34] average crystal size of SAPO-34 samples is 5–20 μm when MOR is used as a template agent. From **Table 2**, the mean crystal size of S1 and S3 were 3.15 and 2.7 μm, respectively. Therefore, our results showed that using TEA or TEAOH as a template in synthesis gel can have a positive effect on crystal size reduction. The results are in agreement with other studies [23,24]. S3 sample with larger width and lower intensity of diffraction peaks illustrated smaller particle size compared to S1. It is concluded that the presence of TEAOH compared to TEA in synthesis gel caused more particle size reduction. The tri-template utilizing both TEA and TEAOH as factors for decreasing the crystal size, resulting in decreasing the crystal size.

Nucleation improvement may be responsible for the crystal size reduction [35]. It could be due to the role of templates as space filling and interaction between the three different types of templates. The greater number of templates causes small space filling around template molecules results in increasing the number of small nuclei.

According to XRD patterns and SEM images, the phase purity and particle size of the samples significantly depend on the nature and number of templates. The S2 sample showed the highest crystallinity (100%) and smallest mean crystal size (0.64 μm).

**Fig. 3.** Contours describing the response surface for relative crystallinity (%) as a function of y(TEAOH) vs. x(TEA).

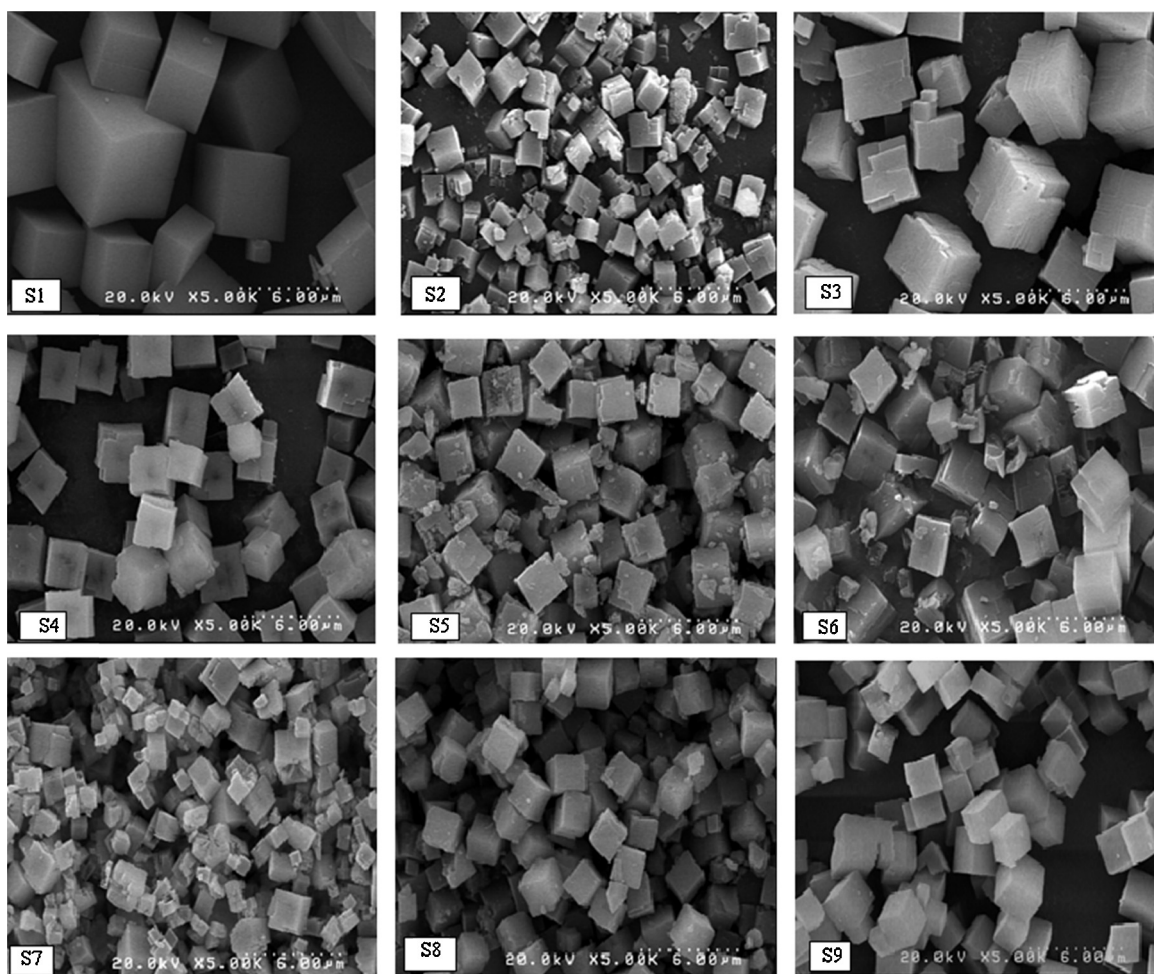


Fig. 4. SEM images of as-synthesized samples.

3.2. Chemical composition and surface area (EDX, BET)

Samples with the best crystallinity and smallest crystal size were selected for EDX, BET and NH₃-TPD analyses. The surface area of samples is given in Table 4. The surface area of pure SAPO-34 can reach up to 650 m²/g [36]. The surface area of prepared samples was very close to pure SAPO-34. Also based on XRD patterns, these samples exhibited high crystallinity without any detectable impurity phase. It can be seen that the surface area of samples did not vary considerably.

The final SAPO-34 compositions with respect to Al, Si and P based on (Al_xP_ySi_z) O₂ formula were obtained by the results of EDX analysis (Table 4). Compared to Si/(Al + P + Si) = 0.091 (%Si content = 9.09) belonging to all starting gels, this ratio in products was higher than 0.091 after crystallization which means the more

amount of Si was incorporated into the framework of SAPO-34 samples and/or remained as amorphous silica phase on extra-framework [27,33]. The amount of the chosen templating agents plays a significant role in silicon incorporation, as well as in the recovery of pure structure with high crystallinity. Therefore, for these samples with high crystallinity, more Si content was incorporated into the framework in the crystallization process. S2 and S4 samples with molar ratios of 0.5 MOR:0.5 TEA:1.0 TEAOH and 1 MOR:0.5 TEA:0.5 TEAOH possessed about 1.1 and 1.2 times increase of the final Si content.

3.3. Acidity (NH₃-TPD, FTIR)

The TPD spectra of NH₃ adsorbed on SAPO-34 samples were used to characterize the acidic properties of samples and the results

Table 4
Physico-chemical properties of synthesized SAPO-34 samples.

Sample	Product composition				Surface area (m ² /g)	Acid strength distribution (%)
		Composition in solid	% Si content	Si incorporation ^a		
S2	Al _{0.5521} Si _{0.1043} P _{0.4110} O ₂	10.05	1.073	625.8	70	30
S3	Al _{0.5301} Si _{0.0964} P _{0.3976} O ₂	9.41	1.034	589.0	48	52
S4	Al _{0.5741} Si _{0.1126} P _{0.4127} O ₂	10.24	1.125	610.3	74	26
S6	Al _{0.5093} Si _{0.094} P _{0.3997} O ₂	9.37	1.030	591.6	42	58
S8	Al _{0.5323} Si _{0.0949} P _{0.3728} O ₂	9.49	1.042	598.9	63	37
S9	Al _{0.5153} Si _{0.0936} P _{0.3911} O ₂	9.36	1.028	578.2	40	60

^a The level of silicon incorporation is defined as the molar ratio of [Si/(Si + Al + P)_{solid}] / [Si/(Si + Al + P)_{gel}].

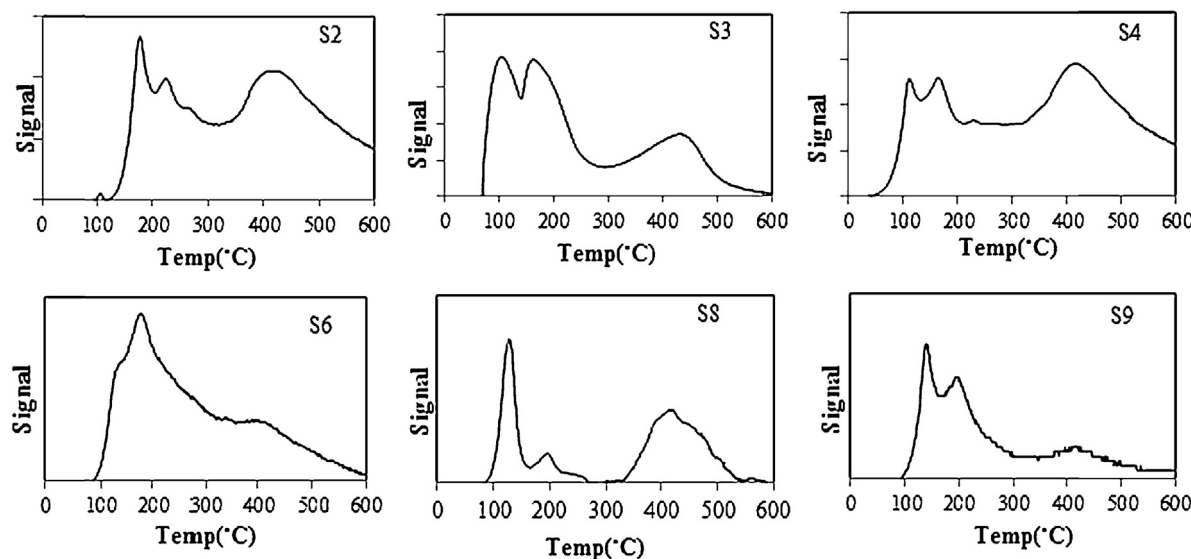


Fig. 5. NH₃-TPD profiles of synthesized SAPO-34 samples.

are shown in **Table 4** and **Fig. 5**. Desorption temperature signifies the strength of acid sites, the stronger acid sites require a higher desorption temperature. The area under the NH₃ desorption curve indicates the amount of ammonia desorbed and the acid strength distribution.

Two desorption peaks, at the range of 150–210 and 370–420 °C as low and high temperature desorption sites were recognized. The first desorption peak of TPD curves, corresponding to weak acid sites, was attributed to the hydroxyl groups (–OH) bounded to the defect sites, i.e. P-OH hydroxyl groups not fully linked to AlO₄ tetrahedral, SiOH and AlOH [37,38]. The samples with lower crystallinity have a higher amount of such kind of these sites.

The weak acid sites, desorb ammonia molecules before reaching to 300 °C [39]. Therefore, these type of acid sites would not be able to adsorb and convert methanol as a less basic molecule at reaction temperature of 410 °C into olefins.

The amount of weak acid sites represented by first peak has no significant effect on MTO performance. For illustrating that weak acid sites is not responsible for methanol conversion to light olefins, Ye et al. [40] performed NH₃-TPD test on deactivated samples after reaction compared with before; the results showed that the second peak of deactivated samples was absolutely missing and the first peak maintained intact after the reaction.

Therefore, the second desorption peak as strong Bronsted acid sites should be activated for MTO reaction. This peak was attributed to the bridging hydroxyl groups, i.e. –SiOHAl–, formed by replacement of phosphorous by silicon [12,41–43]. As is seen in **Table 2** the type and ratio of templates employed in the synthesis affect the distribution of acid sites strength.

There is a consensus that in the case of SAPO-34 molecular sieves, acid sites generation is a consequence of Si incorporation into ALPO framework [44,45]. As shown in **Table 4**, S2, S4 and S8 samples that were prepared by mixing three types of different templates exhibited high distribution of strong acid sites due to higher amount of silicon incorporation.

TPD results agreed with the results from *in situ* FTIR spectra of SAPO-34 samples at the OH-stretching vibration region (**Fig. 6**). The framework vibrations were characteristically similar to those of CHA-structure [14,41,46,47].

There were two adsorption bands at about 3600 and 3625 cm^{−1}, which were assigned to –SiOHAl– groups interacting with the oxygen atoms of the framework and located inside the double-six-rings. These hydroxyl groups are suggested to be the active sites for

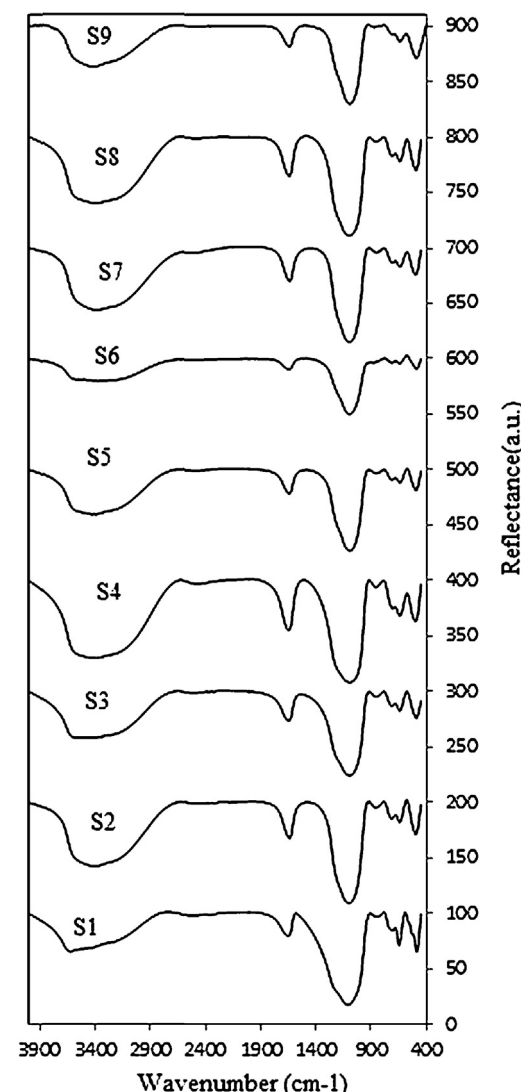


Fig. 6. *In situ* Fourier transform IR spectra of synthesized samples.

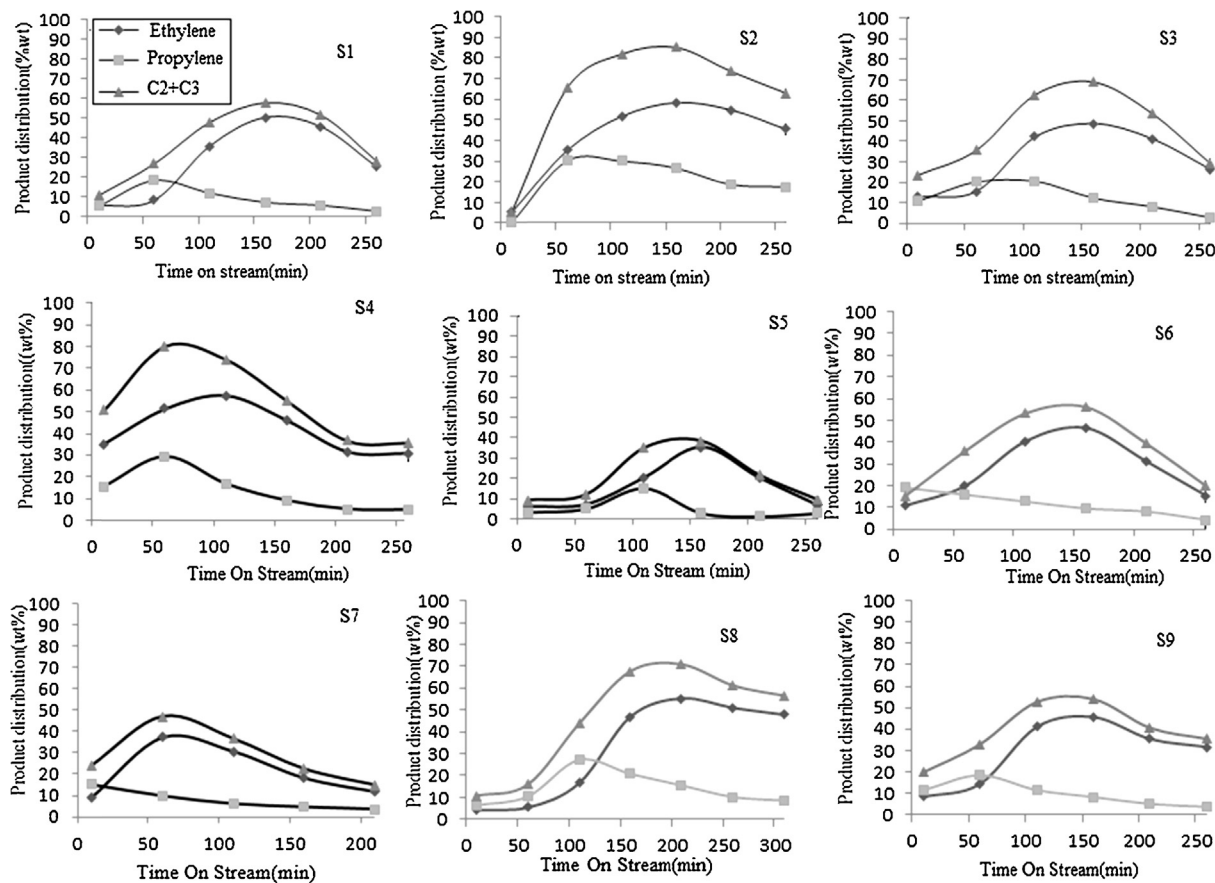


Fig. 7. Products distribution with TOS over synthesized SAPO-34 catalysts (S1–S9) at 410 °C, WHSV of 6.5 h⁻¹.

acid catalyzed reactions [41,46]. S2, S4 and S8 samples indicated higher concentration of the strong acidic hydroxyl groups which also showed higher amount of strong acid sites.

The band at 1635 cm⁻¹ is assigned to the bonding vibrational mode of water weakly adsorbed in the SAPO-34 cages. Bending around 1100 and 730 cm⁻¹ correspond to asymmetric and symmetric stretch of O-P-O. Furthermore, absorption peaks at 640, 580, 530 and 480 cm⁻¹, indicated the bend of double 6-ring, PO₄, AlO₄ and SiO₄, respectively [14,47].

3.4. MTO reaction performance

Catalytic performances of SAPO-34 catalysts synthesized by a mixture of three templates for methanol to olefins (MTO) reaction were tested at 410 °C and WHSV of 6.5 cm⁻¹. For all SAPO-34 catalysts, over 98% conversion of methanol was obtained in MTO reaction. The products distribution of the catalysts with reaction

time on stream (TOS) are shown in Fig. 7. All the prepared samples have catalytic performance at the given condition, but the distribution of products and maximum yield of light olefins varies significantly. Obviously, type of templates and changing the ratio of MOR/TEA/TEAOH affect the products distribution and maximum yield of light olefins.

Maximum yield of ethylene and propylene in methanol conversion reaction over SAPO-34 catalysts are given in Table 5. The maximum yield of ethylene is more than propylene for all catalysts. It is proposed that at reaction temperature 410 °C (>400 °C), propylene and butenes may oligomerize to bigger oligomers, and subsequently formed oligomers could be cracked to ethylene [33].

SAPO-34 catalyst is deactivated to form olefins by two routes. First, deactivation is caused by the formation of coke from the hydrocarbons that entrapped within the cages of SAPO-34 catalyst during the process. Second, it is caused by losing acidity after many cycles of MTO [48]. In methanol to olefin process over SAPO-34

Table 5

Products yield in methanol conversion reaction over SAPO-34 catalysts.

Sample	MOR:TEA:TEAOH	Light olefins yield (wt%)		
		C ₂ H ₄	C ₃ H ₆	C ₂ =C ₃ =
S1	1.5:0.5:0.0	50.50	20.48	70.98
S2	0.5:0.5:1.0	58.41	30.29	88.70
S3	1.5:0.0:0.5	48.78	20.44	69.22
S4	1.0:0.5:0.5	57.38	29.04	86.42
S5	0.5:1.0:0.5	35.46	14.68	50.14
S6	1.0:0.86:0.14	46.54	19.11	65.65
S7	0.28:0.86:0.86	37.13	15.09	52.22
S8	1.0:0.14:0.86	56.35	28.23	84.58
S9	1.72:0.14:0.14	45.60	18.47	64.07

Table 6

Analysis of variance (ANOVA) for the yield of light olefins.

Factor	Sum of squares	df	Mean square	F	p
Model	2268.15	5	453.63	51.50	<0.0001
A – x (TEA content)	417.07	1	417.07	47.35	0.0002
B – y (TEAOH content)	128.78	1	128.78	14.62	0.0065
AB	287.98	1	287.98	32.69	0.0007
A^2	1398.30	1	1398.30	158.74	<0.0001
B^2	117.23	1	117.23	13.31	0.0082
Error	0.14	4	0.035		
Core total	2329.81	12			

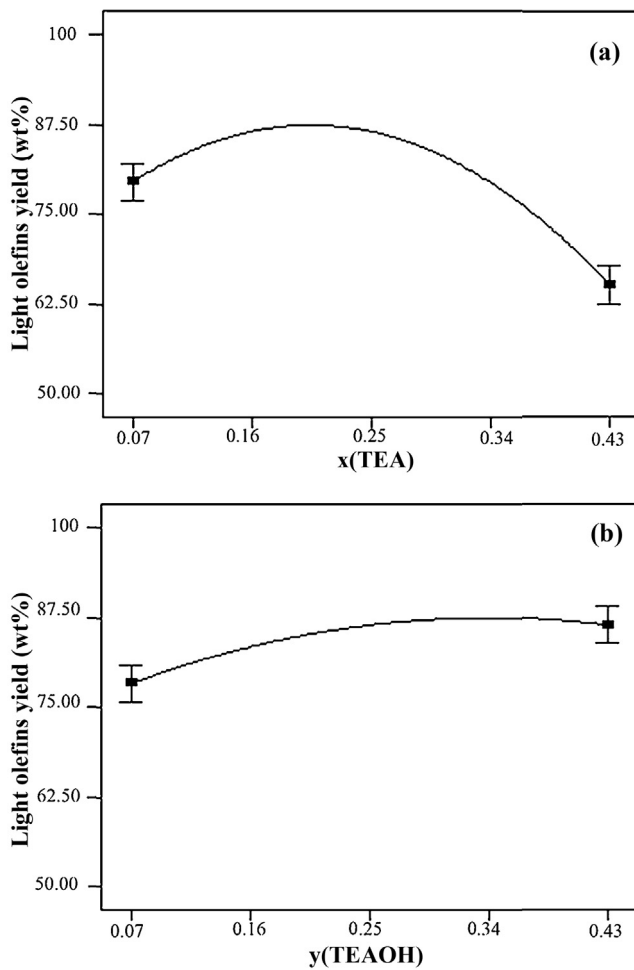


Fig. 8. Main effects of each factor on maximum yield of light olefins (wt%).

catalysts, it is widely accepted that methanol is first dehydrated to DME, then DME can easily be converted to light olefins over strong acid sites of catalysts until the cages inside the SAPO-34 catalysts are occupied by coke. Therefore, after deactivation of the catalysts, conversion of methanol to DME can still take place at the weak acidic sites [10,26,49].

According to Fig. 7, the rate of formation of ethylene and propylene increased with time on stream and reached a maximum. At the first propylene yield reached a maximum then leveled off, whereas

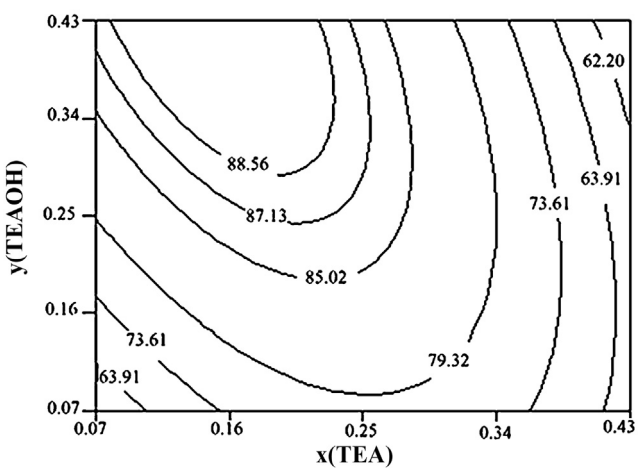


Fig. 9. Contours describing the response surface for light olefins yield (wt%) as a function of y(TEAOH) vs. x(TEA).

Product distribution in MTO reaction is affected by diffusion limitation of propene within pores of SAPO-34 with particle size of $>0.5 \mu\text{m}$ [28]. This observation can be related to the coking effect, which was suggested to be responsible for reduction in pore size of SAPO-34. Coke formation hindered the escape of heavier product molecules from the cage of SAPO-34, so that the production of these molecules suppressed, resulting in increasing yield of lighter alkenes such as ethylene. By the formation of larger hydrocarbons, activity loss of the catalysts became more significant, so the deactivation of the catalysts is caused by diffusional barriers being created rather than loss of active sites [28,50].

Compared with synthesized samples, S2 sample possessed the smallest crystal size about $0.6 \mu\text{m}$. According to Ref. [48,50] the particle size range of $0.5\text{--}1 \mu\text{m}$ is suitable for the process because of minimizing the possibility of inhomogeneous coke distribution. As is seen in Fig. 7, this sample presented the best results in terms of light olefins yield and stability with TOS. So, S2 sample possessed the highest yield of light olefins (88.7 wt%) and the total yield of $\text{C}_2=\text{C}_3$ maintained upper 60% after 250 min. The S4 sample possessed highest yield of light olefins at the first of reaction (about 50%). The highest strong acid sites associated with high surface area of this catalyst that could promote the hydrogen transfer reaction.

From the ANOVA results for light olefins yield (Table 6), the factor A and B and their interactions have statistically significant effects on yield of light olefins. After the ANOVA test, the quadratic polynomial equation for maximum yield of light olefins as a function of actual variables is given in Eq. (6):

$$\begin{aligned} \text{Maximum light olefins yield} = & +37.47561 + 253.87725X_A + 156.25832X_B - 271.52000X_AX_B \\ & - 453.68400X_A^2 - 131.36400X_B^2 \end{aligned} \quad (6)$$

production of ethylene monotonically increased. After activation of the catalyst with a propene pulse, ethylene is able to form stable,

In which X_A and X_B denote actual variables of TEA and TEAOH, respectively. The R^2 value of Eq. (6) is 0.973, indicating a good fitting

between predicted values and experimental data of light olefins yield.

Graphical representations of experimental design are shown in Figs. 8 and 9, to study the effects of variables on maximum yield of light olefins. Although B (TEAOH content) factor is statistically significant, TEA content has the largest effect on yield of light olefins. Fig. 8(a) shows that increase of TEA, changes the light olefins yield in the range of 65–85% while Fig. 8(b) shows that the increasing TEAOH results in increase of light olefins yield in the range of 78–86%. According to Figs. 3 and 9, there is a correlation with relative crystallinity and maximum light olefins yield, so that high crystallinity was in favor of maximum light olefins yield.

The S2, S4 and S8 demonstrated excellent catalytic performance and catalyst stability. Total yields of light olefins were 88.7, 86.42 and 84.58 wt%, respectively (Table 5). These catalysts possessed the highest light olefins yield compared to other samples, including S1 and S3 samples that were prepared using a mixture of two templates. These results may be explained by crystal size, crystallinity, external surface area and strong acid sites.

According to ammonia TPD spectra, S2, S4 and S8 samples indicated high strong acid site distributions (70%, 74% and 63%, respectively). High amount of active sites for these samples resulted in their excellent performance in MTO reaction. In addition, these catalysts have small crystal size, high external surface area and high relative crystallinity that was explained earlier to improve their catalyst activity.

The larger crystal size, limited the ability of the reactant molecules to diffuse in catalyst pores due to increase of diffusion resistance [23]. As a result, the effectiveness of the catalysts increased with the crystal size reduction. The smaller crystal size and high external surface area avoided the formation of heavier hydrocarbons due to rapid outward product diffusion [22].

All the catalysts except S5 and S7 samples exhibited more than 60% yield for light olefins before decreasing on TOS by catalyst deactivation. Lower light olefins yield for S5 and S7 samples can be imputed to their inferior crystallinity as well as lower Si incorporation (Table 4) that was in parallel to lower populations of strong acid sites as compared to other prepared samples.

4. Conclusions

SAPO-34 samples were synthesized hydrothermally using different combinations of MOR/TEA/TEAOH as templates that exhibited different physicochemical properties. The morphology of the samples was similar to cubic shape of typical SAPO-34. It was revealed that using a mixture of three templates in synthesis gel reduced the crystal size of samples. All the synthesized samples indicated SAPO-34 pure phase, distinct in relative crystallinity. The effect of TEA and TEAOH content on relative crystallinity and maximum yield of light olefins was investigated using CCD. According to the ANOVA results TEA content was the most significant factor. The lowest relative crystallinity of synthesized sample was in accordance with the highest amount of TEA content in synthesis gel. The crystal size, crystallinity and acidity strongly affected on light olefins yield of the different catalysts. The catalyst with molar ratios of 0.5 MOR:0.5 TEA:1 TEAOH possessed the highest yield of light olefins (88.7 wt%) due to its smallest crystal size, best crystallinity and highest external surface area.

References

- [1] M.A. Djieugoue, A.M. Prakash, L. Kevan, *J. Phys. Chem. B* 104 (2000) 6452–6461.
- [2] W. Shen, X. Li, Y. Wei, P. Tian, F. Deng, X. Han, X. Bao, *Microporous Mesoporous Mater.* 158 (2012) 19–25.
- [3] F. Cavaní, F. Trifiro, *Catal. Today* 24 (1995) 307–313.
- [4] J. Park, G. Seo, *Appl. Catal. A: Gen.* 356 (2009) 180–188.
- [5] J.W. Park, J.Y. Lee, K.S. Kim, S.B. Hong, G. Seo, *Appl. Catal. A: Gen.* 339 (2008) 36–44.
- [6] S. Wilson, P. Barger, *Microporous Mesoporous Mater.* 29 (1999) 117–126.
- [7] X. Wu, R.G. Anthony, *Appl. Catal. A: Gen.* 218 (2001) 241–250.
- [8] W.J.H. Dehertog, G.F. Froment, *Appl. Catal.* 71 (1991) 153–165.
- [9] C.D. Chang, W.H. Lang, A.J. Silvestri, US Patent 4062905 (1972).
- [10] L. Travalloni, A.C.L. Gomes, A.B. Gaspar, M.A.P. da Silva, *J. Catal.* 263 (2008) 406–412.
- [11] X.C. Wu, M.G. Abraha, R.G. Anthony, *Appl. Catal. A: Gen.* 260 (2004) 63–69.
- [12] G. Sastre, D.W. Lewis, C.R.A. Richard, A. Catlow, *J. Phys. Chem. B* 101 (1997) 5249–5262.
- [13] R. Vomscheid, M. Briend, M.J. Peltre, P.P. Man, D. Barthomeuf, *J. Phys. Chem.* 98 (1994) 9614–9618.
- [14] J. Tan, Zh. Liu, X. Bao, X. Liu, X. Han, C. He, R. Zhai, *Microporous Mesoporous Mater.* 98 (1994) 9614–9618.
- [15] S. Coluccia, L. Marchese, G. Marta, *Microporous Mesoporous Mater.* 30 (1999) 43–56.
- [16] H.V. Heyden, S. Mintova, T. Bein, *Chem. Mater.* 20 (2008) 2956–2963.
- [17] O.B. Vistad, D.E. Akporiaye, F. Taulelle, K.P. Lillerud, *Chem. Mater.* 15 (2003) 1639–1649.
- [18] Y. Hirota, K. Murata, S. Tanaka, N. Nishiyama, Y. Egashira, K. Ueyama, *Mater. Chem. Phys.* 123 (2010) 507–509.
- [19] B.M. Lok, T.R. Cannan, C.A. Messina, *Zeolites* 3 (1983) 282–291.
- [20] H.O. Pastore, S. Coluccia, L. Marchese, *Annu. Rev. Mater. Res.* 35 (2005) 351–395.
- [21] G.Y. Liu, P. Tian, J.Z. Li, D.Z. Zhang, F. Zhou, Z.M. Liu, *Microporous Mesoporous Mater.* 111 (2008) 143–149.
- [22] T. Álvaro-Muñoz, C. Márquez-Álvarez, E. Sastre, *Catal. Today* 179 (2012) 27–34.
- [23] N. Nishiyama, M. Kawaguchi, Y. Hirota, D.V. Vu, Y. Egashira, K. Ueyama, *Appl. Catal. A: Gen.* 362 (2009) 139–199.
- [24] L. Guangyu, T. Peng, L. Zhongmin, Chin. J. Catal. 33 (2012) 174–182.
- [25] S. Askari, R. Halladj, M. Sohrabi, *Rev. Adv. Mater. Sci.* 32 (2012) 83–93.
- [26] Y. Lee, S. Baek, K. Jun, *Appl. Catal. A: Gen.* 329 (2007) 130–136.
- [27] M. Salmasi, Sh. Fatemi, A. Taheri, *J. Ind. Eng. Chem.* 17 (2011) 755–761.
- [28] P. Wang, A. Lv, J. Hu, J. Xu, G. Lu, *Microporous Mesoporous Mater.* 152 (2012) 178–184.
- [29] B.M. Lok, C.A. Messina, R.L. Patton, R.T. Gajek, T.R. Cannan, E.M. Flanigen, U.S. Patent No. 4440871 (1984).
- [30] J.B. Casady, R.W. Johnson, *Solid-State Electron.* 39 (1996) 1409–1422.
- [31] Y. Hang, M. Qu, S.B. Ukkusuri, *Energy Build.* 43 (2011) 988–994.
- [32] D. Bas, I.H. Boyaci, *J. Food Eng.* 78 (2007) 836–845.
- [33] A.M. Prakash, S. Unnikrishnan, *J. Chem. Soc. Faraday Trans.* 90 (1994) 2291–2296.
- [34] L. Marchese, A. Frache, E. Gianotti, G. Martra, M. Causa, S. Coluccia, *Microporous Mesoporous Mater.* 30 (1999) 145–153.
- [35] B. Topuz, E.E. Oral, H. Kalipcilar, *J. Porous Mater.* 20 (2013) 1491–1500.
- [36] J.W. Yoon, S.H. Jhung, Y.H. Kim, S.E. Park, J.S. Chang, *Bull. Korean Chem. Soc.* 26 (2005) 558–562.
- [37] B. Parlitz, E. Schreier, H.L. Zubowa, R. Eckelt, E. Lieschke, R. Fricke, *J. Catal.* 155 (1995) 1–11.
- [38] M. Popova, Ch. Minchev, V. Kanazirev, *Appl. Catal. A: Gen.* 169 (1998) 227–235.
- [39] A. Izadbakhsh, F. Farhadi, F. Khorasheh, S. Sahebdelfar, M. Asadi, Y.Z. Feng, *Appl. Catal. A: Gen.* 364 (2009) 48–56.
- [40] L. Ye, F. Cao, W. Ying, D. Fang, Q. Sun, *J. Porous Mater.* 18 (2011) 225–232.
- [41] B. Zibrowius, E. Löffler, M. Hunger, *Zeolites* 12 (1992) 167–174.
- [42] S. Ashtekar, S.V.V. Chilukuri, D.K. Chakrabarty, *J. Phys. Chem.* 98 (1994) 4878–4883.
- [43] E. Dumitriu, A. Azzouz, V. Hulea, D. Lutic, H. Kessler, *Microporous Mater.* 10 (1997) 1–12.
- [44] S. Svelle, S. Aravindhan, M. Bjørgen, K.P. Lillerud, S. Kolboe, I.M. Dahl, U. Olsbye, *J. Catal.* 241 (2006) 243–259.
- [45] R.B. Borade, A. Clearfield, *J. Mol. Catal.* 88 (1994) 249–265.
- [46] S.A. Zubkov, L.M. Kustov, V.B. Kazansky, I. Girnus, R. Fricke, *J. Chem. Soc. Faraday Trans.* 87 (1991) 897–900.
- [47] K.-H. Schnabel, R. Fricke, I. Girnus, E. Jahn, E. Löffler, B. Parlitz, C. Peuker, *J. Chem. Soc. Faraday Trans.* 87 (1991) 3569–3574.
- [48] D.S. Wragg, A. Grønvold, A. Voronov, P. Norby, H. Fjellvag, *Microporous Mesoporous Mater.* 173 (2013) 166–174.
- [49] M.J. Van Niekerk, J.C.Q. Fletcher, C.T. O'Connor, *Appl. Catal. A: Gen.* 138 (1996) 135–145.
- [50] I.M. Dahl, R. Wendelbo, A. Andersen, D. Akporiaye, H. Mostad, T. Fuglerud, *Microporous Mesoporous Mater.* 29 (1999) 159–171.